Improved ink-jet-printed CdSe quantum dot light-emitting diodes with minimized hole transport layer erosion

Tang, Haodong; Jia, Siqi; Ding, Shihao; Liu, Pai; Ma, Jingrui; Xiao, Xiangtian; Qu, Xiangwei; Liu, Haochen; Yang, Hongcheng; Xu, Bing; Chen, Wei; Li, Guangyu; Pikramenou, Zoe; Anthony, Carl; Wang, Kai; Sun, Xiao Wei

DOI:
10.1021/acsaelm.1c00210

Document Version
Publisher's PDF, also known as Version of record

Citation for published version (Harvard):
Tang, H, Jia, S, Ding, S, Liu, P, Ma, J, Xiao, X, Qu, X, Liu, H, Yang, H, Xu, B, Chen, W, Li, G, Pikramenou, Z, Anthony, C, Wang, K & Sun, XW 2021, 'Improved ink-jet-printed CdSe quantum dot light-emitting diodes with minimized hole transport layer erosion', *ACS Applied Electronic Materials*, vol. 3, no. 7, pp. 3005-3014. https://doi.org/10.1021/acsaelm.1c00210

ACS APPLIED ELECTRONIC MATERIALS

pubs.acs.org/acsaelm Article

Improved Ink-Jet-Printed CdSe Quantum Dot Light-Emitting Diodes with Minimized Hole Transport Layer Erosion

Haodong Tang,[#] Siqi Jia,[#] Shihao Ding, Pai Liu, Jingrui Ma, Xiangtian Xiao, Xiangwei Qu, Haochen Liu, Hongcheng Yang, Bing Xu, Wei Chen, Guangyu Li, Zoe Pikramenou, Carl Anthony, Kai Wang,* and Xiao Wei Sun*

Cite This: *ACS Appl. Electron. Mater.* 2021, 3, 3005−3014 Read Online

ACCESS | Metrics & More | Article Recommendations | Supporting Information

ABSTRACT: Ink-jet printing is a promising deposition technology, which is capable of large-area fabrication and mask-free patterning. For ink-jet-printed quantum dot (QD) light-emitting diodes (LEDs), the QDs are commonly dissolved in a mixture of solvent and thickener ink system. However, the hole transport layer could be eroded by this QD ink, leading to a rough surface morphology and resulting in the leakage of carriers and low device performance. This phenomenon was first and directly observed by using an atomic force microscope and a cross-sectional scanning electron microscope. We, therefore, redesigned the annealing process of the hole transport layer to achieve an optimized smooth surface with a reduced number of defects for ink-jet-printed QD LEDs (QLEDs). Optimized morphology brings back a maximum luminance of over 30,000 cd/m^2 and an external quantum efficiency of 7.52% for the ink-jet-printed red QLEDs using CdSe QDs, which are comparable to those of the spin-coated device. Moreover, the operation lifetime of the ink-jet-printed device is also enhanced by the restored surface morphology. An enhanced T_{50} lifetime of the ink-jet-printed device at 1000 cd/m^2 is improved from 26 to 127 h, which converted to a long T_{50} lifetime of 8013 h, when operated at 100 cd/m^2.

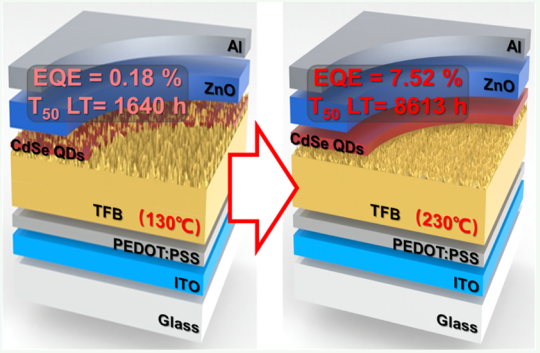

KEYWORDS: *ink-jet printing, annealing process, hole transporting layer, erosion, QLED, stability*

INTRODUCTION

Quantum dots (QDs) are emerging semiconductor nanocrystals with extremely small sizes of several nanometers. Benefiting from the smaller size than the Bohr radius of electrons, QDs have exhibited attractive properties including sharp emission bandwidth, size-dependent emission wavelength, solution processability, and high emission efficiency.[1−3] These unique advantages have made QDs especially popular in high-quality display areas aiming at true color,[4,5] large area,[6−8] and flexible display.[9,10] With the superiority of vivid colors, low energy consumption, and relevant low cost of fabrication, electroluminescence (EL) QD light-emitting diodes (QLEDs) have shown their potential to become an emerging display technology in recent years.[11−15] QLEDs are constructed of electrodes, a hole injection layer, a hole transport layer (HTL), a QD layer, and an electron transport layer (ETL). One of the most commonly used fabrication methods of QLEDs is spin-coating, which is of low cost and does not require expensive equipment or vacuum and materials could be flatly deposited layer by layer. However, the shortcoming is also obvious; the limited scale of fabrication and a massive waste of materials make this technology more suitable in laboratories rather than in industrial production. A large-scale and cost-efficient fabrication process is necessary for the commercialization of QLEDs.

Blade coating,[16,17] slot-die printing,[18] and spray-coating[19,20] technologies have been studied, aiming at large-area fabrication of optoelectrical devices. However, they have difficulties in thickness control and coating precision. Moreover, the material waste is high. Thus, these technologies are not suitable for industrial fabrication for now.

Ink-jet printing is an attractive technology for the fabrication of electrical circuits, detectors, and wearable electronic devices[21−25] due to its low-cost, no-contact process and maskless on-demand patterning in contrast with other film-deposition technologies.[26,27] Since Jabbour et al. first reported the fabrication of QLEDs by ink-jet printing in 2009,[28] the efficiency and stability of QLEDs by ink-jet

Received: March 4, 2021
Accepted: May 17, 2021
Published: June 1, 2021

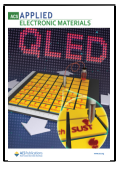

https://doi.org/10.1021/acsaelm.1c00210
ACS Appl. Electron. Mater. 2021, 3, 3005−3014

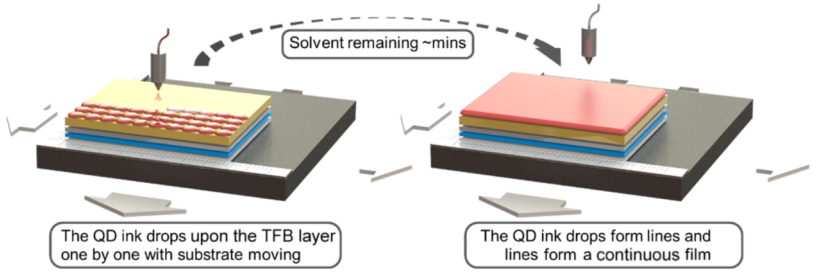

Figure 1. Schematic demonstration of the film-formation process during ink-jet printing.

printing have been improved steadily.[29−32] Necessarily, during the ink-jet printing process, the surface tension and viscosity of the ink must match the requirement of the printing system to ensure the successful dropping of a continuous single droplet, which limits the choice of the ink composition. Considering the solubility of QDs, researchers have developed different ink systems to maintain both the solubility of QDs and the viscosity of ink.[29,31] The multiple-solvent ink system is one of the most successful strategies.[25,32,33] By mixing a thickener (with high viscosity) with another solvent (with good solubility of QDs), this type of ink satisfies both the requirements and produced some good studies with high resolution,[25] high luminance,[29] and high efficiency.[34] However, these fabricated devices still have a long way to go compared with spin-coated ones, especially when considering the device efficiency and the lifetime.

One of the problems lies in the interface between the QD layer and the HTL. For spin coating, the solvents of the QD and HTL are orthogonal, which can avoid the problem of redissolution, while in the ink-jet printing process, the ink system cannot avoid introducing aromatic compounds (as a thickener) to meet the requirement of viscosity.[35] The aromatic chemicals such as cyclohexylbenzene (CHB) could result in redissolution or erosion of the HTL containing the benzene ring, For example, the commonly used HTL material, aiming at long-lifetime devices, poly[(9,9-dioctyl-fluorenyl-2,7-diyl)-*alt*-(4,4′-(*N*-(4-butylphenyl) (TFB) is such a compound. Moreover, because of the sequential ink printing process, the ink would normally stay for several minutes on the HTL (as shown in Figure 1). This redissolution and erosion of the HTL could destroy the interface, trigger a sharp decrease in the efficiency of charge injection and transport, and lead to low device performance.

In this work, we studied how the annealing temperature of the HTL affects the final device performance of ink-jet-printed QLEDs. A commonly used QLED structure (ITO/poly(3,4-ethylenedioxythiophene) polystyrene sulfonate (PEDOT:PSS)/TFB/CdSe QD/ZnO/Al) was adopted, wherein TFB is the HTL. Also, a well-documented ink system mixed with CHB and decane in a ratio of 10:1 was applied in this work.[34] Necessarily, the surface tension and viscosity of the ink are listed in Table S1. The annealing temperature of TFB was set from 130 (which is the common choice for TFB in spin-coated QLEDs) to 280 °C to gain a whole picture of the temperature effect.[35] The enhanced resistance property of TFB to QD ink was first analyzed by absorption spectra; also, the effects of the variation of annealing temperature on the smoothed morphology of the TFB film were observed by atomic force microscopy (AFM) and scanning electron microscopy (SEM). Our ink-jet-printed red QLEDs with an optimized annealing temperature of TFB exhibit enhanced device performance, achieving a maximum external quantum efficiency (EQE) of 7.52% and a current efficiency (CE) of 10 cd/A. The luminance under 6 V bias was enhanced from 446 to 19,669 cd/m^2 (maximum luminance was over 30,000 cd/m^2 under 8 V bias) by increasing the annealing temperature of TFB from 130 to 230 °C. Also, the capacitance−voltage ($C-V$) analysis confirmed the enhanced charge injection and recombination in the optimized device. The T_{50} lifetime with an initial luminance of 1000 cd/m^2 under atmospheric conditions was enhanced from 26 to 127 h. This work demonstrates the importance of the interfacial morphology of the HTL in the ink-jet printing process. Stronger resistance of the HTL to the ink will bring significant enhancement to the device performance. This simple, feasible yet efficient method could be generalized in industrial fabrication and show its potential in helping commercialize the applications of ink-jet-printed QLEDs.

RESULTS AND DISCUSSION

First, we have evaluated the solvent resistance of TFB films by measuring the absorption spectrum before and after rinsing with CHB, which is the major component in QD ink for ink-jet printing. The TFB films were spin-coated and annealed at different temperatures for 15 min. Blue lines in Figure 2 show the absorbance curves for the as-fabricated

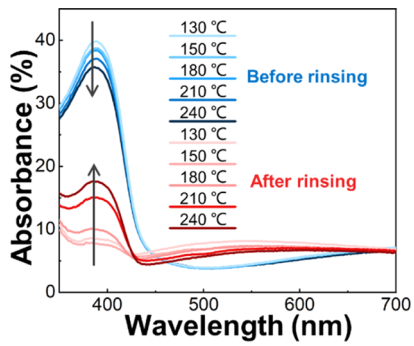

Figure 2. Absorption spectra of spin-coated TFB films before (blue lines) and after (red lines) rinsing of the QD ink.

TFB films after different annealing processes. The first exciton absorption peaks of TFB located at 387 nm can be observed.[38] The decreased intensity of the first exciton absorption peak (blue lines) indicated an increased degree of disorder of TFB when annealed at higher temperature.[39,40] The thermogravimetric analysis (TGA) shown in Figure S1a has confirmed that the decreased absorption of light is not attributed to the decomposition of TFB until heated up to 300 °C. However, after being rinsed with CHB, all samples exhibited an obvious decrease in the absorption peak, which

https://doi.org/10.1021/acsaelm.1c00210
ACS Appl. Electron. Mater. 2021, 3, 3005−3014

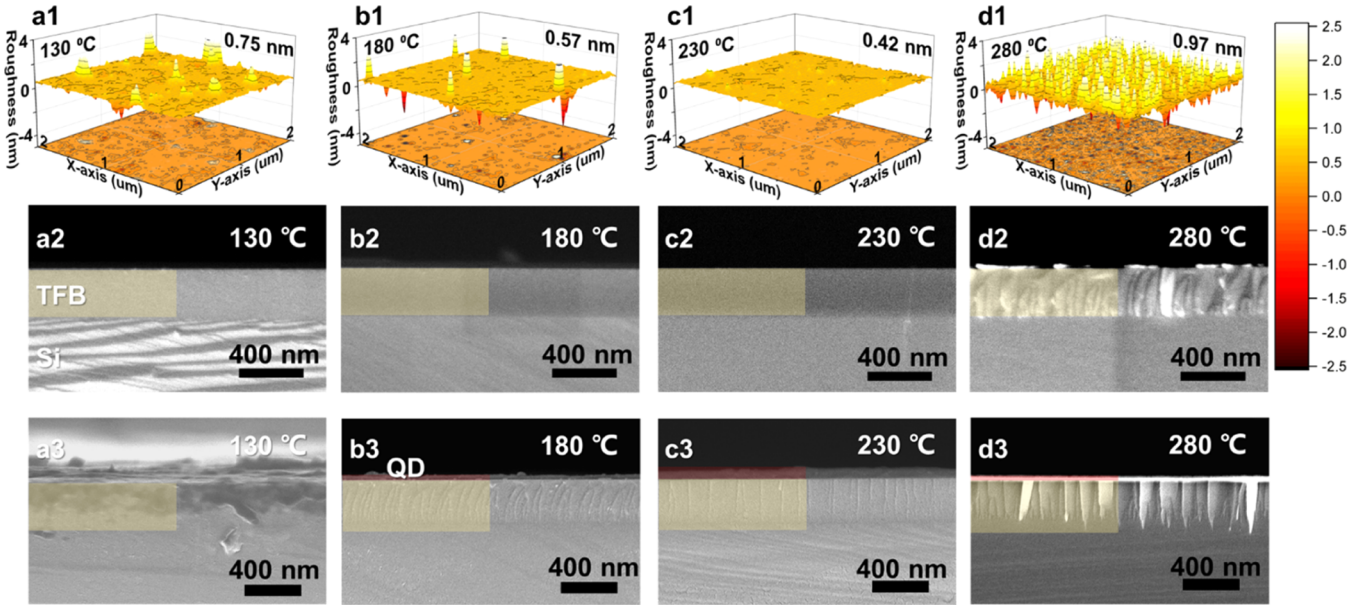

Figure 3. AFM results of spin-coated TFB films annealed at different temperatures from 130 °C up to 280 °C (a1−d1). The RMS roughness is marked on the top-right corner of each figure. An enhanced surface morphology is observed when the annealing temperature is increased from 130 to 230 °C. A minimum surface roughness of 0.42 nm is achieved when the film is annealed at 230 °C. However, the surface roughness is sharply increased when annealed at 280 °C. Furthermore, the cross-sectional SEM images of TFB films (a2−d2) show the potential crystallization of TFB when overheated. Moreover, after spin-coating the QD ink on these TFB films, the cross-sectional SEM images show different degrees of erosion (a3−d3).

was caused by the erosion or redissolution of TFB. Samples with higher temperature annealing processes showed less damage with stronger resistance to the solvent. The increased resistance to the solvent resulted in more amount of TFB remaining on the substrate. All these features revealed higher absorption intensity at a wavelength of 387 nm.

Furthermore, characterizations including AFM and SEM were performed to show the surface and interfacial morphology of these TFB films. The TFB films were spin-coated on silicon wafers to facilitate SEM analysis. For better visualization of the cross-section, a lower spin speed was used to achieve a thicker film thickness (~300 nm) while maintaining good surface roughness. Then, these samples were annealed at 130, 180, 230, and 280 °C. Figure S2 shows the top-view SEM images of these samples. We can see that there are some bright spots on the surface of all films. These spots (formed by accumulated electrons during the imaging of SEM) indicate less conductive areas, which could result in uneven distribution of current in QLEDs and would affect the efficiency of electron−hole recombination. The difference in the surface morphology is responsible for the different densities of bright spots in TFB samples.

Moreover, the 2D AFM results provided in Figure S3 show the difference in roughness. Here, the AFM data are replotted as 3D figures (Figure 3a1−d1) with a normalized scale bar for better comparison. As the annealing temperature increases from 130 to 180 °C, a decreased number of pinholes and islands could be observed on TFB films. Eventually, for the TFB film annealed at 230 °C, a super flat surface morphology was achieved with a low root-mean-square (RMS) roughness of 0.42 nm. This decreased level of roughness could be attributed to different levels of degradation and recrystallization during the annealing process over the glass-transition temperature.[39] However, for the overheated sample annealed at 280 °C, the sharply increased level of degradation and recrystallization resulted in a pinhole and island-rich morphology with an RMS roughness of 0.97 nm. In the temperature range from 130 to 280 °C, TFB goes through a continuous heat absorption process (refer to differential scanning calorimetry (DSC) results in Figure S1b). The initial heat absorption point (~90 °C) is defined as the glass-transition temperature of the material. Our TFB revealed a constant glass transition or recrystallization process from 130 to 280 °C. This process would cause the redistribution of TFB chains and result in different morphologies with various degrees of roughness.

Furthermore, Figure 3a2−d2 shows the cross-sectional SEM images of these samples. The TFB films annealed below 230 °C exhibit no cracks or crystal-like structures. Nevertheless, a clear crystalline structure could be observed for the overheated (280 °C) sample. The massive number of cracks is responsible for the increased RMS roughness shown in Figure 3d1. Then, the interaction between QD ink and these TFB films was studied. Figure 3a3−d3 shows the cross-sectional SEM images of these TFB films after the ink-jet printing of QDs. At a lower annealing temperature of 130 °C, not only was the TFB film destroyed but also the QDs did not form a continuous film because of the uneven surface and erosion. When the annealing temperature of TFB was increased to 180 and 230 °C, the strong erosion was replaced by slight infiltration through the cracks inside the TFB layer. TFB chains were redistributed, compactly stacked [supported by the Fourier transform infrared (FTIR) results in Figure S4], and formed a flatter surface morphology. Reduced pinholes and islands made the TFB films capable of preventing the erosion by QD ink. Also, the QD films were successfully deposited on these TFB films annealed at higher temperatures. Moreover, the thickest QD layer was achieved on the TFB film annealed at 230 °C. However, the infiltration of QD ink exposed the small cracks inside the

https://doi.org/10.1021/acsaelm.1c00210
ACS Appl. Electron. Mater. 2021, 3, 3005−3014

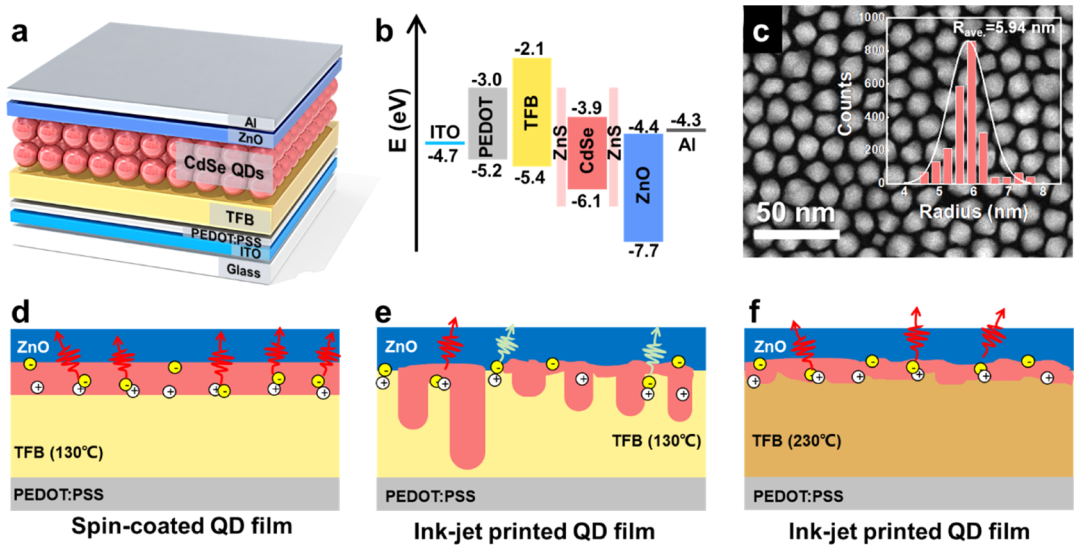

Figure 4. Device structure we selected for the optimization of the TFB layer (a). This is a well-designed band structure with a modified injection barrier (b). Also, the HR-TEM and size distribution analysis of QDs show the good quality of synthesized CdSe QDs with an average radius of 5.94 nm (c). Three kinds of devices were designed and fabricated with different deposition methods of QDs and different annealing temperatures of TFB. The spin-coated device was selected as a pristine group with no erosion of the TFB layer (d). The ink-jet-printed device with TFB annealed at 130 °C suffered from huge erosion of printed ink drops (e), resulting in increased leaked current and decreased device performance. By increasing the annealing temperature of TFB to 230 °C (f), the erosion of QD ink was suppressed, resulting in optimized EL efficiency.

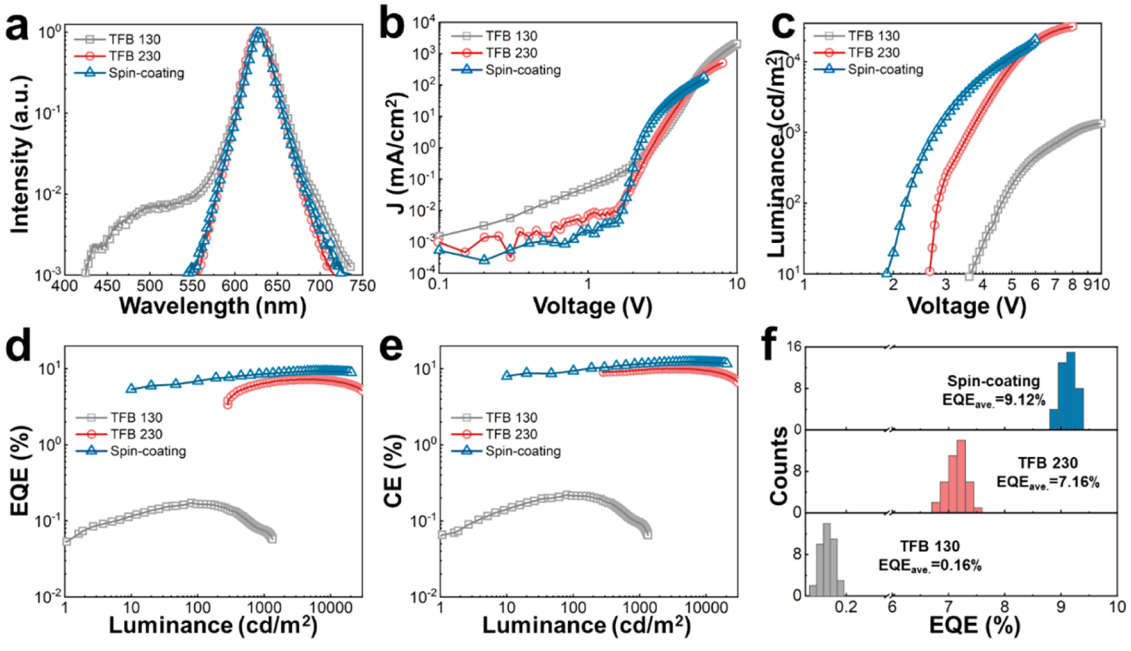

Figure 5. Normalized EL spectra of the fabricated devices including the spin-coated device and ink-jet-printed devices with TFB annealed at 130 and 230 °C (a). Current density analyses of these devices show the detailed carrier transport properties of these devices (b). Also, the luminance−voltage curves show different turn-on voltages (the voltage when luminance reaches 10 cd/m^2) and luminance outputs of these devices (c). EQE and CE curves versus luminance analysis show the EL efficiency of these devices (d,e). Finally, this enhancement of EQE is repeatable according to our experiments (f).

TFB layer (Figure 3b2,c3). Fewer cracks mean fewer channels for carrier leakage and less chance of carrier recombination in the TFB layer. However, the crystal-like structures in 280 °C-annealed TFB (Figure 3d2) provided sufficient channels for the infiltration of QD ink, resulting in another type of erosion shown in Figure 3d3. The imperfect interfacial morphology caused by cracks, crystal-like structures, and erosions would surely decrease the device performance dramatically, especially limiting the operation lifetime of the ink-jet-printed QLEDs.

Several QLED devices were designed and fabricated to analyze the possible changes brought by the increased annealing temperature of TFB. A typical device structure ITO/PEDOT:PSS/TFB/CdSe:ZnS QDs/ZnO/Al was adopted (Figure 4a). The band structure of the QLED is shown in Figure 4b. Holes would be injected from ITO, through

https://doi.org/10.1021/acsaelm.1c00210
ACS Appl. Electron. Mater. 2021, 3, 3005−3014

Table 1. Device Performance

device	peak wavelength (nm)	luminance @6 V (cd/m^2)	EQE_{max} (%)	CE_{max} (cd/A)	T_{50} lifetime @L_0 = 1000 cd/m^2 (h)	T_{50} lifetime @L_0 = 100 cd/m^2 (h)
ink-jet printed 130 °C	629.9	446.3	0.18	0.22	26	1640
ink-jet printed 230 °C	628.2	19,668.8	7.52	10.03	127	8013
spin-coated 130 °C	627.5	20,503.4	9.32	12.33		

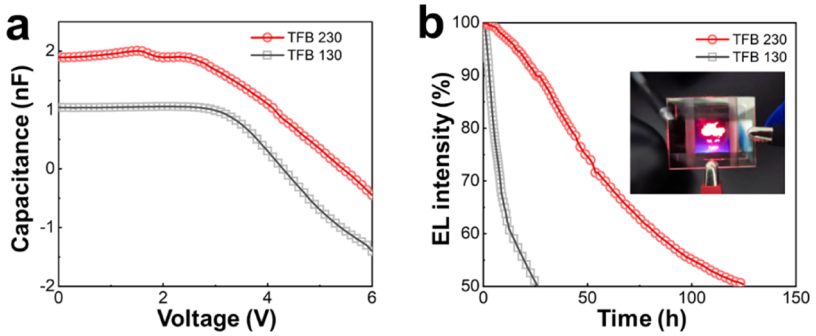

Figure 6. (a) *C*−*V* analysis of the ink-jet-printed devices at 1k Hz. (b) Lifetime of ink-jet-printed devices with an initial luminance of 1000 cd/m^2. The inset shows the mask-free patterned ink-jet-printed device.

PEDOT:PSS and TFB, into QDs. On the other side, electrons would be injected from Al, through ZnO, into QDs and then radiatively recombined with holes. The emitted light would be extracted from a transparent ITO substrate. High-resolution transmission electron microscopy (HR-TEM) was performed to analyze the particle size of CdSe:ZnS QDs (Figure 4c). Uniformly distributed CdSe:ZnS QDs with an average radius of 5.94 nm were achieved. Figure 4d−f shows the schematics of the differences in morphology and interface between spin-coated and ink-jet-printed devices. We used the spin-coated device as the control group where the spin-coated QDs have no damage to the TFB layer. However, as shown in Figure 3, different degrees of damage could be observed when ink-jet-printed QDs were deposited on the TFB layer. These cracks and tunnels could provide a channel for carriers recombining outside the QD layer, resulting in the emission of the HTL layer. This would decrease the device performance and should be avoided. By increasing the annealing temperature to 230 °C, the infiltration of ink-jet-printed QDs could be suppressed and the emission of the HTL layer could also be eliminated. Thus, the electron−hole pairs could be confined inside the QD layer, and the efficiency of radiative recombination is strongly enhanced. Moreover, extra evidence has been provided in the FTIR spectroscopy results shown in Figure S4. The newly appeared peaks at ∼2900 cm^{-1} are attributed to bonding and reconstruction of TFB chains when annealed at a higher temperature.

The EL spectra of our QLEDs given in Figure 4d−f are shown in Figure 5a. All of these devices showed a sharp red-light emission with a central wavelength near 628 nm and a full wavelength at half maximum of 27 nm. To better expose the weak emission signal, the vertical axis is set as a log scale. Interestingly, a wide side emission from 430 to 550 nm due to TFB[36,37] can be seen in the figure for the ink-jet-printed device with TFB annealed at 130 °C. This is hard evidence for the carriers leaked through the QD layer and recombined in the TFB layer. However, when the annealing temperature was increased to 230 °C, the side emission of TFB was suppressed because of the intact TFB layer as shown in the cross-sectional SEM images. Likewise, the higher current density of the ink-jet-printed device annealed at 130 °C below 2 V could also support our guess of massive leaked carriers through the eroded TFB layer (Figure 5b). It can be seen from Figure 5c that ink-jet-printed QLED based on TFB annealed at 230 °C gives similar luminance performance to the spin-coated device. The efficiency of radiative recombination has been greatly improved. A large number of leaked carriers delayed the turn-on voltage up to 3.6 V for the ink-jet-printed device with TFB annealed at a lower temperature. After increasing the annealing temperature of TFB up to 230 °C, the turn-on voltage is lowered down to 2.7 V. However, this turn-on point is still higher than that of the spin-coated device (1.9 V). This difference in turn-on voltage is caused by the different number of leakage tunnels in these fabricated QLEDs. The spin-coated device has the least tunnels for leakage, benefited from the orthogonal solvent system. However, the ink-jet-printed QLED with TFB annealed at 130 °C has most of the leaked carriers because of the eroded TFB and the discontinuous deposited QD layer. The ink-jet-printed QLED with the optimized TFB annealing process has minimized the erosion, resulting in fewer leaked carriers and lower turn-on voltage. Figure 5d,e shows the EQE and CE of these devices. The efficiency of ink-jet-printed QLEDs at a modified annealing temperature of TFB is comparable to that of a spin-coated device, as shown in Table 1.

The carrier dynamics in the ink-jet-printed devices were characterized by *C*−*V* measurement (Figure 6a). The capacitance of QLEDs is directly related to the change in charge quantity in QLED devices. Therefore, it is an effective way to evaluate the carrier injection, transporting, and recombination and charge balance in QLED devices. The device capacitance is calculated by

$$C = \frac{dQ}{dU} = \frac{dQ_{in} + dQ_{trap} - dQ_r}{dV} \quad (1)$$

https://doi.org/10.1021/acsaelm.1c00210
ACS Appl. Electron. Mater. 2021, 3, 3005−3014

where Q_{in}, Q_{trap}, and Q_r are the injected carriers for the electrode charging process, trapped carriers, and recombined carriers, respectively.[41]

The carriers accumulated in different layers of the QLED device generated this capacitance. At initial capacitance or when the voltage is small (<2 V), the geometry capacitance is presented, which exhibits the number of leaked carriers. These leaked carriers have not participated in the injection, trapping, or recombination processes. Higher geometry capacitance of the ink-jet-printed device with 230 °C-annealed TFB indicates more injected carriers for the electrode charging process. Therefore, there were fewer channels for leaked current. Minimized erosion of TFB by QD ink led to this improvement. The erosion of TFB resulted in a massive leakage of electrons, and these leaked electrons could recombine with holes inside the TFB layer under higher voltage. The $C-V$ curves at higher voltage indicate the carrier dynamics of accumulation and recombination. The recombination of carriers could cause the decrease in capacitance, and on the other hand, an increased number of injected carriers could also enhance the capacitance. The accumulation of carriers and increased capacitance were not observed in devices with TFB annealed at 130 °C, which was caused by massive leakage channels of carriers. However, these channels were suppressed in a device with TFB annealed at 230 °C. A slight increase below 2 V showed the accumulation of carriers inside the device. The earlier turning point, which means where the recombination of carriers has already occurred in the majority, for the device with TFB annealed at 230 °C, indicates higher efficiency of radiative recombination. This also explains the reason for the higher EQE compared with the ink-jet-printed device with TFB annealed at 130 °C.

Finally, the lifetimes of these two devices were measured with an initial luminance of 1000 cd/m^2. The currents applied on both devices are fixed, according to the luminance−current density scan data, to maintain the stable EL intensity. Photodetectors were attached with both devices to monitor the change in luminance. The result is given in Figure 6b. With modified interfacial morphology, suppressed carrier leakage, and enhanced EQE, the EL lifetime of the optimized device reached 127 h. Compared with the control group, the lifetime was only 26 h due to the bad carrier control and device efficiency. These T_{50} lifetimes with L_0 = 1000 cd/m^2 were converted to the T_{50} lifetimes with L_0 = 100 cd/m^2 according to eq 2,[36] shown in Table 1.

$$L^n \times t = \text{constant} \quad (2)$$

where L is the initial luminance, t is the measured time, and n is the acceleration factor. The T_{50} lifetimes were recalculated to be 1640 and 8613 h for the ink-jet-printed devices before and after the optimization of the annealing temperature of TFB, respectively.

The optimized surface morphology and thickness of the QD layer should be majorly responsible for the enhanced device performance because of the suppressed leakage of carriers. Furthermore, the improved uniformity of carrier distribution could slow down the speed of degradation for ink-jet-printed devices, while the majority of degradation in the device level comes from the accumulation of carriers, resulting in the accumulation of heat and current, then inducing the shape changing of layers or even the breakdown of materials. The ink-jet-printed device with TFB annealed at 230 °C has greatly improved both the surface and interfacial morphology between the TFB and QD layer, bringing back the high EL efficiency and long operation lifetime to ink-jet-printed QLED.

CONCLUSIONS

The low efficiency and lifetime of ink-jet-printed QLED devices with CHB−decane ink systems are attributed to the bad surface morphology of the HTL layer. The surface roughness is caused by the erosion effect when QD ink is dropped on the TFB layer. To solve this, we have increased the annealing temperature of TFB from 130 to 230 °C. The increased annealing temperature of TFB protected it from erosion by the QD ink and suppressed the leakage of carriers in the fabricated QLEDs. Eventually, devices with QDs ink-jet printed on TFB annealed at 230 °C exhibited enhanced luminance of over 30,000 cd/m^2 under 8 V bias. We achieved a repeatable enhancement of EQE for ink-jet-printed devices from 0.18 to 7.52% when the annealing temperature of TFB was increased from 130 to 230 °C. Also, the T_{50} lifetime of the optimized device at an initial luminance of 1000 cd/m^2 was enhanced to 127 h, which was 8013 h when the initial luminance was 100 cd/m^2.

EXPERIMENTAL SECTION

List of Chemicals. PEDOT:PSS was purchased from Xi'an Polymer Light Technology Corp. and TFB was purchased from Lumtec, dissolved in chlorobenzene (Aladdin, 99.5%). The QDs and ZnO nanoparticles were synthesized by Plank Ink. The QDs were dissolved in decane (Sigma, 99%) with a concentration of 20 mg/mL. Then, the QDs/decane solution was mixed with CHB (Aladdin, 97%) with a ratio of 1:10 to fabricate the QD ink for ink-jet printing and rinsing. ZnO nanoparticles were dissolved in ethanol (Aladdin, 99.8%) with a concentration of 20 mg/mL.

Fabrication of TFB Films. The TFB films were spin-coated on silicon substrates. Before the fabrication, the substrates were cleaned with acetone, ethanol, and deionized water, using an ultrasonic cleaner. TFB was dissolved in chlorobenzene with a concentration of 15 mg/mL. The spin-coating process was set at 2000 rpm for 45 s. After spin-coating, all samples were annealed on a hot plate at different temperatures for 15 min. The rinsing process was performed by a simple drop and spin-off process. One milliliter of ink was dropped on the TFB film to fulfill the TFB film for 30 s. Then, the ink was spin off with a speed of 4000 rpm.

Characterization of Materials and Films. The transmission spectra of the TFB films were acquired using a PerkinElmer LAMBDA 950 spectrophotometer. TGA and DSC were performed by Discovery TGA and Discovery DSC, respectively. The AFM characterization was performed through Asylum Research MFP-3D-SA, and SEM was performed using Zeiss GeminiSEM 300. FTIR was performed using a Nicolet spectrometer (TENSOR27, Burkeer, Germany). HR-TEM was performed by using FEI Titan Themis G2 working on high-angle annular dark-field scanning TEM images. The characterization of surface tension was carried out using a surface tension meter (JK99B, Powereach, China). The viscosity of QD ink was measured using a Brookfield rotational viscometer (DV3T).

Fabrication of the Ink-Jet-Printed QLED. The QLED was fabricated on patterned ITO glasses. The glasses were cleaned with ethanol using an ultrasonic cleaner for 20 min. Then, the substrates were dried using nitrogen and hydrophilically treated in a UV−ozone chamber for 15 min. The cleaned and hydrophilic-treated substrates were then taken for further device fabrication processes. The PEDOT:PSS and TFB layers were spin-coated in a fume hood at 3000 rpm and 1500 acc, respectively. The substrate was annealed at 120 °C for 10 min before the spin-coating of TFB. The annealing temperature was designed as 130, 180, 230, and 280 °C for 15 min. Then, the substrates were taken to a glovebox for ink-jet printing.

https://doi.org/10.1021/acsaelm.1c00210
ACS Appl. Electron. Mater. 2021, 3, 3005−3014

The ink-jet printing of QD inks on the TFB layer was performed by using a Microfab JETLAB 2 printer equipped with a piezoelectric-driven inkjet nozzle (diameter: 40 μm) in the glovebox. The accuracy of the motorized stage is 5 μm. The electric-driven voltage of the inkjet printer is shown in Figure S5. The ink-jet printing process took 2 min to fabricate a QD film with 12 mm length and 8 mm width to cover the four emission pixels in one substrate. Then, the film was annealed at 120 °C for 15 min to remove the ink as much as possible. Then, the ZnO ETL layer was deposited by spin-coating at 2500 rpm and 1250 acc, followed by annealing at 100 °C for 10 min. The top electrodes were fabricated by heat evaporation of aluminum for 120 nm. The device was then packaged using UV glue in a glovebox, protecting the materials from moisture and oxygen.

Characterization of the Ink-Jet-Printed QLED. The EL spectra, current density, luminance, EQE, and CE of the device were characterized using an XPQY-EQE-350-1100 QLED characterization system (Guangzhou Xi Pu Optoelectronics Technology Co., Ltd.) combined with a GPS-4P-SL integrated sphere (Labsphere) and an S7031-1006 photodetector (Hamamatsu Photonics). Furthermore, the $C-V$ analysis was performed using an HP4284A impedance analyzer with a frequency of 1k Hz. The lifetime analysis was carried out using a steady-current source to drive the QLEDs, combined with a photodetector to monitor the change in luminance.

■ ASSOCIATED CONTENT

Supporting Information

The Supporting Information is available free of charge at https://pubs.acs.org/doi/10.1021/acsaelm.1c00210.

Thermal analysis including TGA and DSC; morphology analysis of TFB films including top-view SEM and 2D-AFM results; FTIR results; driving voltage of the ink-jet printer; and analysis of QD ink and device comparison (PDF)

■ AUTHOR INFORMATION

Corresponding Authors

Kai Wang − *Key Laboratory of Energy Conversion and Storage Technologies, Southern University of Science and Technology, Ministry of Education, Shenzhen 518055, China; Guangdong-Hong Kong-Macao Joint Laboratory for Photonic-Thermal-Electrical Energy Materials and Devices, Guangdong University Key Laboratory for Advanced Quantum Dot Displays and Lighting, Shenzhen Key Laboratory for Advanced Quantum Dot Displays and Lighting, and Department of Electrical and Electronic Engineering, Southern University of Science and Technology, Shenzhen 518055, China;* orcid.org/0000-0003-0443-6955; Email: wangk@sustc.edu.cn

Xiao Wei Sun − *Key Laboratory of Energy Conversion and Storage Technologies, Southern University of Science and Technology, Ministry of Education, Shenzhen 518055, China; Guangdong-Hong Kong-Macao Joint Laboratory for Photonic-Thermal-Electrical Energy Materials and Devices, Guangdong University Key Laboratory for Advanced Quantum Dot Displays and Lighting, Shenzhen Key Laboratory for Advanced Quantum Dot Displays and Lighting, and Department of Electrical and Electronic Engineering, Southern University of Science and Technology, Shenzhen 518055, China; Shenzhen Planck Innovation Technology Pte., Ltd., Shenzhen 518112, China;* orcid.org/0000-0002-2840-1880; Email: sunxw@sustech.edu.cn

Authors

Haodong Tang − *Key Laboratory of Energy Conversion and Storage Technologies, Southern University of Science and Technology, Ministry of Education, Shenzhen 518055, China; Guangdong-Hong Kong-Macao Joint Laboratory for Photonic-Thermal-Electrical Energy Materials and Devices, Guangdong University Key Laboratory for Advanced Quantum Dot Displays and Lighting, Shenzhen Key Laboratory for Advanced Quantum Dot Displays and Lighting, and Department of Electrical and Electronic Engineering, Southern University of Science and Technology, Shenzhen 518055, China; College of Engineering and Physical Sciences, University of Birmingham, Birmingham B15 2TT, U.K.;* orcid.org/0000-0002-5632-5096

Siqi Jia − *Key Laboratory of Energy Conversion and Storage Technologies, Southern University of Science and Technology, Ministry of Education, Shenzhen 518055, China; Guangdong-Hong Kong-Macao Joint Laboratory for Photonic-Thermal-Electrical Energy Materials and Devices, Guangdong University Key Laboratory for Advanced Quantum Dot Displays and Lighting, Shenzhen Key Laboratory for Advanced Quantum Dot Displays and Lighting, and Department of Electrical and Electronic Engineering, Southern University of Science and Technology, Shenzhen 518055, China; Key Laboratory of Automobile Materials, Ministry of Education, Department of Materials Science and Engineering, Jilin University, Changchun 130025, China*

Shihao Ding − *Key Laboratory of Energy Conversion and Storage Technologies, Southern University of Science and Technology, Ministry of Education, Shenzhen 518055, China; Guangdong-Hong Kong-Macao Joint Laboratory for Photonic-Thermal-Electrical Energy Materials and Devices, Guangdong University Key Laboratory for Advanced Quantum Dot Displays and Lighting, Shenzhen Key Laboratory for Advanced Quantum Dot Displays and Lighting, and Department of Electrical and Electronic Engineering, Southern University of Science and Technology, Shenzhen 518055, China; Shenzhen Planck Innovation Technology Pte., Ltd., Shenzhen 518112, China*

Pai Liu − *Key Laboratory of Energy Conversion and Storage Technologies, Southern University of Science and Technology, Ministry of Education, Shenzhen 518055, China; Guangdong-Hong Kong-Macao Joint Laboratory for Photonic-Thermal-Electrical Energy Materials and Devices, Guangdong University Key Laboratory for Advanced Quantum Dot Displays and Lighting, Shenzhen Key Laboratory for Advanced Quantum Dot Displays and Lighting, and Department of Electrical and Electronic Engineering, Southern University of Science and Technology, Shenzhen 518055, China*

Jingrui Ma − *Key Laboratory of Energy Conversion and Storage Technologies, Southern University of Science and Technology, Ministry of Education, Shenzhen 518055, China; Guangdong-Hong Kong-Macao Joint Laboratory for Photonic-Thermal-Electrical Energy Materials and Devices, Guangdong University Key Laboratory for Advanced Quantum Dot Displays and Lighting, Shenzhen Key Laboratory for Advanced Quantum Dot Displays and Lighting, and Department of Electrical and Electronic Engineering, Southern University of Science and Technology, Shenzhen 518055, China*

https://doi.org/10.1021/acsaelm.1c00210
ACS Appl. Electron. Mater. 2021, 3, 3005−3014

Xiangtian Xiao − *Key Laboratory of Energy Conversion and Storage Technologies, Southern University of Science and Technology, Ministry of Education, Shenzhen 518055, China; Guangdong-Hong Kong-Macao Joint Laboratory for Photonic-Thermal-Electrical Energy Materials and Devices, Guangdong University Key Laboratory for Advanced Quantum Dot Displays and Lighting, Shenzhen Key Laboratory for Advanced Quantum Dot Displays and Lighting, and Department of Electrical and Electronic Engineering, Southern University of Science and Technology, Shenzhen 518055, China*

Xiangwei Qu − *Key Laboratory of Energy Conversion and Storage Technologies, Southern University of Science and Technology, Ministry of Education, Shenzhen 518055, China; Guangdong-Hong Kong-Macao Joint Laboratory for Photonic-Thermal-Electrical Energy Materials and Devices, Guangdong University Key Laboratory for Advanced Quantum Dot Displays and Lighting, Shenzhen Key Laboratory for Advanced Quantum Dot Displays and Lighting, and Department of Electrical and Electronic Engineering, Southern University of Science and Technology, Shenzhen 518055, China*

Haochen Liu − *Key Laboratory of Energy Conversion and Storage Technologies, Southern University of Science and Technology, Ministry of Education, Shenzhen 518055, China; Guangdong-Hong Kong-Macao Joint Laboratory for Photonic-Thermal-Electrical Energy Materials and Devices, Guangdong University Key Laboratory for Advanced Quantum Dot Displays and Lighting, Shenzhen Key Laboratory for Advanced Quantum Dot Displays and Lighting, and Department of Electrical and Electronic Engineering, Southern University of Science and Technology, Shenzhen 518055, China*

Hongcheng Yang − *Key Laboratory of Energy Conversion and Storage Technologies, Southern University of Science and Technology, Ministry of Education, Shenzhen 518055, China; Guangdong-Hong Kong-Macao Joint Laboratory for Photonic-Thermal-Electrical Energy Materials and Devices, Guangdong University Key Laboratory for Advanced Quantum Dot Displays and Lighting, Shenzhen Key Laboratory for Advanced Quantum Dot Displays and Lighting, and Department of Electrical and Electronic Engineering, Southern University of Science and Technology, Shenzhen 518055, China*

Bing Xu − *Key Laboratory of Energy Conversion and Storage Technologies, Southern University of Science and Technology, Ministry of Education, Shenzhen 518055, China; Guangdong-Hong Kong-Macao Joint Laboratory for Photonic-Thermal-Electrical Energy Materials and Devices, Guangdong University Key Laboratory for Advanced Quantum Dot Displays and Lighting, Shenzhen Key Laboratory for Advanced Quantum Dot Displays and Lighting, and Department of Electrical and Electronic Engineering, Southern University of Science and Technology, Shenzhen 518055, China; Shenzhen Planck Innovation Technology Pte., Ltd., Shenzhen 518112, China*

Wei Chen − *Key Laboratory of Energy Conversion and Storage Technologies, Southern University of Science and Technology, Ministry of Education, Shenzhen 518055, China; Guangdong-Hong Kong-Macao Joint Laboratory for Photonic-Thermal-Electrical Energy Materials and Devices, Guangdong University Key Laboratory for Advanced Quantum Dot Displays and Lighting, Shenzhen Key Laboratory for Advanced Quantum Dot Displays and Lighting, and Department of Electrical and Electronic Engineering, Southern University of Science and Technology, Shenzhen 518055, China;* orcid.org/0000-0001-9550-0523

Guangyu Li − *Key Laboratory of Automobile Materials, Ministry of Education, Department of Materials Science and Engineering, Jilin University, Changchun 130025, China;* orcid.org/0000-0001-6723-7895

Zoe Pikramenou − *College of Engineering and Physical Sciences, University of Birmingham, Birmingham B15 2TT, U.K.;* orcid.org/0000-0002-6001-1380

Carl Anthony − *College of Engineering and Physical Sciences, University of Birmingham, Birmingham B15 2TT, U.K.*

Complete contact information is available at: https://pubs.acs.org/10.1021/acsaelm.1c00210

Author Contributions

#H.T and S.J. have contributed equally to this work.

Notes

The authors declare no competing financial interest.

■ ACKNOWLEDGMENTS

H.T. and S.J. have contributed equally to this work. We would like to acknowledge support from the Ministry of Science and Technology of China (nos. 2016YFB0401702 and 2017YFE0120400), the National Natural Science Foundation of China (nos. 61674074, 61875082, and 61405089), the Guangdong Province's Key R&D Program: Micro-LED Display and Ultra-high Brightness Micro-display Technology (no. 2019B010925001); Environmentally Friendly Quantum Dots Luminescent Materials (no. 2019B010924001), the Guangdong Basic and Applied Basic Research Foundation (no. 2019A1515110437), the Guangdong University Key Laboratory for Advanced Quantum Dot Displays and Lighting (no. 2017KSYS007), the Shenzhen Innovation Project (no. JCYJ20180305180629908), the Guangdong Youth Innovative Talents Project (no. 2018KQNCX228), and the Shenzhen Peacock Team Project (no. KQTD2016030111203005). The authors would like to acknowledge the technical support from Dongsheng He and Yang Qiu in SUSTech CRF.

■ REFERENCES

(1) Peng, X.; Manna, L.; Yang, W.; Wickham, J.; Scher, E.; Kadavanich, A.; Alivisatos, A. P. Shape Control of Cdse Nanocrystals. *Nature* **2000**, *404*, 59−61.

(2) Chen, O.; Zhao, J.; Chauhan, V. P.; Cui, J.; Wong, C.; Harris, D. K.; Wei, H.; Han, H.-S.; Fukumura, D.; Jain, R. K.; Bawendi, M. G. Compact High-Quality Cdse-Cds Core-Shell Nanocrystals with Narrow Emission Linewidths and Suppressed Blinking. *Nat. Mater.* **2013**, *12*, 445−451.

(3) Kagan, C. R.; Lifshitz, E.; Sargent, E. H.; Talapin, D. V. Building Devices from Colloidal Quantum Dots. *Science* **2016**, *353*, aac5523.

(4) Lee, K.-H.; Han, C.-Y.; Kang, H.-D.; Ko, H.; Lee, C.; Lee, J.; Myoung, N.; Yim, S.-Y.; Yang, H. Highly Efficient, Color-Reproducible Full-Color Electroluminescent Devices Based on Red/Green/Blue Quantum Dot-Mixed Multilayer. *ACS Nano* **2015**, *9*, 10941−10949.

(5) Ji, T.; Jin, S.; Zhang, H.; Chen, S.; Sun, X. W. Full Color Quantum Dot Light-Emitting Diodes Patterned by Photolithography Technology. *J. Soc. Inf. Disp.* **2018**, *26*, 121−127.

(6) Qasim, K.; Chen, J.; Xu, F.; Wu, J.; Li, Z.; Lei, W.; Cui, Y.; Xia, J. Large-Area Quantum-Dot Light Emitting Diode Arrays with Zno Nanoparticles as Electron Transport/Injection Layer. *Sci. Adv. Mater.* **2014**, *6*, 2625−2631.
(7) Li, X.; Hu, B.; Du, Z.; Wu, Y.; Jiang, L. Asymmetric Wettability Interfaces Induced a Large-Area Quantum Dot Microstructure toward High-Resolution Quantum Dot Light-Emitting Diodes. *ACS Appl. Mater. Interfaces* **2019**, *11*, 28520−28526.
(8) Dai, X.; Deng, Y.; Peng, X.; Jin, Y. Quantum-Dot Light-Emitting Diodes for Large-Area Displays: Towards the Dawn of Commercialization. *Adv. Mater.* **2017**, *29*, 1607022.
(9) Pan, J.; Chen, J.; Huang, Q.; Khan, Q.; Liu, X.; Tao, Z.; Lei, W.; Xu, F.; Zhang, Z. Flexible Quantum Dot Light Emitting Diodes Based on Zno Nanoparticles. *RSC Adv.* **2015**, *5*, 82192−82198.
(10) Li, F.; Shen, J.; Liu, X.; Cao, Z.; Cai, X.; Li, J.; Ding, K.; Liu, J.; Tu, G. Flexible Qled and Opv Based on Transparent Polyimide Substrate with Rigid Alicyclic Asymmetric Isomer. *Org. Electron.* **2017**, *51*, 54−61.
(11) Yang, X.; Mutlugun, E.; Zhao, Y.; Gao, Y.; Leck, K. S.; Ma, Y.; Ke, L.; Tan, S. T.; Demir, H. V.; Sun, X. W. Solution Processed Tungsten Oxide Interfacial Layer for Efficient Hole-Injection in Quantum Dot Light-Emitting Diodes. *Small* **2014**, *10*, 247−252.
(12) Li, X.; Zhao, Y.-B.; Fan, F.; Levina, L.; Liu, M.; Quintero-Bermudez, R.; Gong, X.; Quan, L. N.; Fan, J.; Yang, Z.; Hoogland, S.; Voznyy, O.; Lu, Z.-H.; Sargent, E. H. Bright Colloidal Quantum Dot Light-Emitting Diodes Enabled by Efficient Chlorination. *Nat. Photonics* **2018**, *12*, 159−164.
(13) Zhang, C.; Wang, S.; Li, X.; Yuan, M.; Turyanska, L.; Yang, X. Core/Shell Perovskite Nanocrystals: Synthesis of Highly Efficient and Environmentally Stable $FAPbBr_3/CsPbBr_3$ for LED Applications. *Adv. Funct. Mater.* **2020**, *30*, 1910582.
(14) Wang, H.; Gong, X.; Zhao, D.; Zhao, Y.-B.; Wang, S.; Zhang, J.; Kong, L.; Wei, B.; Quintero-Bermudez, R.; Voznyy, O.; Shang, Y.; Ning, Z.; Yan, Y.; Sargent, E. H.; Yang, X. Multi-functional Molecular Modifier Enabling Efficient Large-Area Perovskite Light-Emitting Diodes. *Joule* **2020**, *4*, 1977−1987.
(15) Wu, Q.; Cao, F.; Wang, H.; Kou, J.; Zhang, Z. H.; Yang, X. Promoted Hole Transport Capability by Improving Lateral Current Spreading for High-Efficiency Quantum Dot Light-Emitting Diodes. *Adv. Sci.* **2020**, *7*, 2001760.
(16) Zeng, Q.; Chen, Z.; Liu, Y.; Guo, T. Efficient larger size white quantum dots light emitting diodes using blade coating at ambient conditions. *Org. Electron.* **2021**, *88*, 106021.
(17) Yu, H.; Zhang, J.; Long, T.; Xu, M.; Feng, H.; Zhang, L.; Liu, S.; Xie, W. Efficient All-Blade-Coated Quantum Dot Light-Emitting Diodes through Solvent Engineering. *J. Phys. Chem. Lett.* **2020**, *11*, 9019−9025.
(18) Chen, W.; Tang, H.; Li, N.; Scheel, M. A.; Xie, Y.; Li, D.; Körstgens, V.; Schwartzkopf, M.; Roth, S. V.; Wang, K.; Sun, X. W.; Müller-Buschbaum, P. Colloidal PbS quantum dot stacking kinetics during deposition via printing. *Nanoscale Horiz.* **2020**, *5*, 880−885.
(19) Han, D.; Khan, Y.; Gopalan, K.; Pierre, A.; Arias, A. C. Emission Area Patterning of Organic Light-Emitting Diodes (OLEDs) via Printed Dielectrics. *Adv. Funct. Mater.* **2018**, *28*, 1802986.
(20) Chen, W.; Tang, H.; Chen, Y.; Heger, J. E.; Li, N.; Kreuzer, L. P.; Xie, Y.; Li, D.; Anthony, C.; Pikramenou, Z.; Ng, K. W.; Sun, X. W.; Wang, K.; Müller-Buschbaum, P. Spray-deposited PbS colloidal quantum dot solid for near-infrared photodetectors. *Nano Energy* **2020**, *78*, 105254.
(21) YousefiAmin, A.; Killilea, N. A.; Sytnyk, M.; Maisch, P.; Tam, K. C.; Egelhaaf, H. J.; Langner, S.; Stubhan, T.; Brabec, C. J.; Rejek, T.; Halik, M.; Poulsen, K.; Niehaus, J.; Köck, A.; Heiss, W. Fully Printed Infrared Photodetectors from PbS Nanocrystals with Perovskite Ligands. *ACS Nano* **2019**, *13*, 2389−2397.
(22) Choi, M.-J.; Kim, Y.; Lim, H.; Alarousu, E.; Adhikari, A.; Shaheen, B. S.; Kim, Y. H.; Mohammed, O. F.; Sargent, E. H.; Kim, J. Y.; Jung, Y. S. Tuning Solute-Redistribution Dynamics for Scalable Fabrication of Colloidal Quantum-Dot Optoelectronics. *Adv. Mater.* **2019**, *31*, 1805886.
(23) Derby, B. Inkjet Printing of Functional and Structural Materials: Fluid Property Requirements, Feature Stability, and Resolution. *Annu. Rev. Mater. Res.* **2010**, *40*, 395−414.
(24) Peng, X.; Yuan, J.; Shen, S.; Gao, M.; Chesman, A. S. R.; Yin, H.; Cheng, J.; Zhang, Q.; Angmo, D. Perovskite and Organic Solar Cells Fabricated by Inkjet Printing: Progress and Prospects. *Adv. Funct. Mater.* **2017**, *27*, 1703704.
(25) Yang, P.; Zhang, L.; Kang, D. J.; Strahl, R.; Kraus, T. High-Resolution Inkjet Printing of Quantum Dot Light-Emitting Microdiode Arrays. *Adv. Opt. Mater.* **2019**, *8*, 1901429.
(26) Singh, M.; Haverinen, H. M.; Dhagat, P.; Jabbour, G. E. Inkjet Printing-Process and Its Applications. *Adv. Mater.* **2010**, *22*, 673−685.
(27) Jia, S.; Li, G.; Liu, P.; Cai, R.; Tang, H.; Xu, B.; Wang, Z.; Wu, Z.; Wang, K.; Sun, X. W. Highly Luminescent and Stable Green Quasi-2d Perovskite-Embedded Polymer Sheets by Inkjet Printing. *Adv. Funct. Mater.* **2020**, *30*, 1910817.
(28) Haverinen, H. M.; Myllylä, R. A.; Jabbour, G. E. Inkjet Printing of Light Emitting Quantum Dots. *Appl. Phys. Lett.* **2009**, *94*, 073108.
(29) Tang, P.; Xie, L.; Xiong, X.; Wei, C.; Zhao, W.; Chen, M.; Zhuang, J.; Su, W.; Cui, Z. Realizing 22.3% Eqe and 7-Fold Lifetime Enhancement in Qleds Via Blending Polymer Tfb and Cross-Linkable Small Molecules for a Solvent-Resistant Hole Transport Layer. *ACS Appl. Mater. Interfaces* **2020**, *12*, 13087−13095.
(30) Liu, Y.; Li, F.; Xu, Z.; Zheng, C.; Guo, T.; Xie, X.; Qian, L.; Fu, D.; Yan, X. Efficient All-Solution Processed Quantum Dot Light Emitting Diodes Based on Inkjet Printing Technique. *ACS Appl. Mater. Interfaces* **2017**, *9*, 25506−25512.
(31) Xie, L.; Xiong, X.; Chang, Q.; Chen, X.; Wei, C.; Li, X.; Zhang, M.; Su, W.; Cui, Z. Inkjet-Printed High-Efficiency Multilayer Qleds Based on a Novel Crosslinkable Small-Molecule Hole Transport Material. *Small* **2019**, *15*, 1900111.
(32) Han, Y. J.; Kim, D. Y.; An, K.; Kang, K.-T.; Ju, B.-K.; Cho, K. H. Sequential Improvement from Cosolvents Ink Formulation to Vacuum Annealing for Ink-Jet Printed Quantum-Dot Light-Emitting Diodes. *Materials* **2020**, *13*, 4754.
(33) Li, Z.; Li, P.; Chen, G.; Cheng, Y.; Pi, X.; Yu, X.; Yang, D.; Han, L.; Zhang, Y.; Song, Y. Ink Engineering of Inkjet Printing Perovskite. *ACS Appl. Mater. Interfaces* **2020**, *12*, 39082−39091.
(34) Xiong, X.; Wei, C.; Xie, L.; Chen, M.; Tang, P.; Shen, W.; Deng, Z.; Li, X.; Duan, Y.; Su, W.; Zeng, H.; Cui, Z. Realizing 17.0% External Quantum Efficiency in Red Quantum Dot Light-Emitting Diodes by Pursuing the Ideal Inkjet-Printed Film and Interface. *Org. Electron.* **2019**, *73*, 247−254.
(35) Park, Y.; Park, Y.; Lee, J.; Lee, C. Simulation for Forming Uniform Inkjet-Printed Quantum Dot Layer. *J. Appl. Phys.* **2019**, *125*, 065304.
(36) Xiang, C.; Wu, L.; Lu, Z.; Li, M.; Wen, Y.; Yang, Y.; Liu, W.; Zhang, T.; Cao, W.; Tsang, S.-W.; Shan, B.; Yan, X.; Qian, L. High Efficiency and Stability of Ink-Jet Printed Quantum Dot Light Emitting Diodes. *Nat. Commun.* **2020**, *11*, 1646.
(37) Lee, C.-Y.; Kuo, Y.-P.; Chen, P.-Y.; Lu, H.-H.; Lin, M. Y. Influence of Annealing Temperature on Weak-Cavity Top-Emission Red Quantum Dot Light Emitting Diode. *Nanomaterials* **2019**, *9*, 1639.
(38) Renzi, W.; Cordeiro, N. J. A.; de Santana, H.; Costa, M. F.; da Silva, M. A. T.; Laureto, E.; Duarte, J. L. Exploring the Experimental Photoluminescence, Raman and Infrared Responses and Density Functional Theory Results for Tfb Polymer. *Synth. Met.* **2018**, *236*, 24−30.
(39) Zhang, X.; Xia, Y.; Friend, R. H.; Silva, C. Sequential Absorption Processes in Two-Photon-Excitation Transient Absorption Spectroscopy in a Semiconductor Polymer. *Phys. Rev. B: Condens. Matter Mater. Phys.* **2006**, *73*, 245201.
(40) Han, Y. J.; An, K.; Kang, K. T.; Ju, B. K.; Cho, K. H. Optical and Electrical Analysis of Annealing Temperature of High-Molecular

https://doi.org/10.1021/acsaelm.1c00210
ACS Appl. Electron. Mater. 2021, 3, 3005−3014

Weight Hole Transport Layer for Quantum-Dot Light-Emitting Diodes. *Sci. Rep.* **2019**, *9*, 10385.
(41) Zhang, L.; Nakanotani, H.; Adachi, C. Capacitance-Voltage Characteristics of a 4,4 '-Bis (N-Carbazole)Styryl Biphenyl Based Organic Light-Emitting Diode: Implications for Characteristic Times and Their Distribution. *Appl. Phys. Lett.* **2013**, *103*, 093301.

https://doi.org/10.1021/acsaelm.1c00210
ACS Appl. Electron. Mater. 2021, 3, 3005−3014